

Quantum and Thermal Phase Slips in Superconducting Niobium Nitride (NbN) Ultrathin Crystalline Nanowire: Application to Single Photon Detection

Cécile Delacour,^{*,†} Bernard Pannetier,[†] Jean-Claude Villegier,[‡] and Vincent Bouchiat[†]

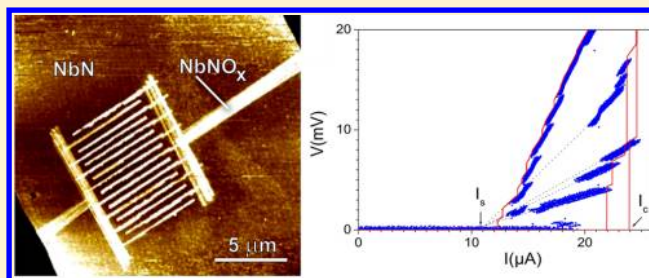
[†]Institut Néel, CNRS et Université Joseph Fourier, BP 166, F-38042 Grenoble, France

[‡]Institut Nanoscience et Cryogénie (INAC), UMR-E CEA/UJF, CEA Grenoble, F-38054 Grenoble, France

Supporting Information

ABSTRACT: We present low-temperature electronic transport properties of superconducting nanowires obtained by nanolithography of 4-nm-thick niobium nitride (NbN) films epitaxially grown on sapphire substrate. Below 6 K, clear evidence of phase slippages is observed in the transport measurements. Upon lowering the temperature, we observe the signatures of a crossover between a thermal and a quantum behavior in the phase slip regimes. We find that phase slips are stable even at the lowest temperatures and that no hotspot is formed. The photoresponse of these nanowires is measured as a function of the light irradiation wavelength and temperature and exhibits a behavior comparable with previous results obtained on thicker films.

KEYWORDS: Superconducting nanowire, phase slip center, superconducting single photon detector, niobium nitride ultrathin films, local anodic oxidation, atomic force microscope



Superconducting nanowires have been the subject of intense experimental studies these past few years on both applied and fundamental levels. On the applied level, these systems appear to be adequate devices for photon detection,¹ reaching the single photon detection threshold² with high bandwidth³ and limited dead time.⁴ On the fundamental level, a better understanding of the activation mechanisms for quantum phase slips has shown a crossover from thermal activation toward a quantum regime at the lowest temperatures,^{5,6} offering interesting perspectives for the realization of quantum information devices.⁷

Among superconducting nanowires, the technology based on NbN ultrathin films appeared to be very promising route and has been favored for the implementation of single photon detectors^{8–11} as the relatively high transition temperature of NbN makes these photonic devices operable at 4 K.

Following these advances, we present a comprehensive experimental study of low-temperature transport properties of niobium nitride (NbN) nanowires obtained using different high-resolution lithography techniques and etching of 4-nm-thick epitaxially grown films.

The NbN nanowires were obtained by lithography and etching of 4-nm-thick NbN crystalline films in a similar fashion as in the previous study focused on the demonstration of single photon sensitivity.⁸ The films are deposited on sapphire substrate having the R-plane orientation of atomically polished quality (3 or 4 in. diameter) sapphire¹² (see the Supporting Information). High-resolution transmission electron micro-

scope imaging (HRTEM) acquired on a thinned cross section of these films confirms the good crystalline nature of the NbN film (Figure 1a) which achieves heteroepitaxy over the R-plane sapphire. The nanowires are fabricated by using two lithography steps: striplines of 20 μm width are first realized by optical DUV photolithography followed by SF_6 plasma etching. Second the nanowire width is further reduced and shaped in a meander line geometry (Figure 1b) using high-resolution lithography processes, either based on conventional electron beam lithography (EBL) or on local anodization⁸ with an atomic force microscope (AFM). The latter process provides several advantages besides its sub-10 nm lateral resolution¹³ such as offering further protection against aging given by the AFM-induced oxide layer passivating the nanowire sides. This technique also allows to keep a rather straight and uniform wire edge. Indeed the roughness of the wire edges is about few nanometers, much smaller than the typical width of the nanowire (>50 nm). This sample property is particularly important for keeping locally uniform superconducting properties (critical current density and transition temperature) and ensures consistent sensitivity and detection efficiency along the nanowire.

We measure electron transport properties of the NbN nanowire in a four-probe geometry from room temperature

Received: March 16, 2012

Revised: May 29, 2012

Published: June 13, 2012

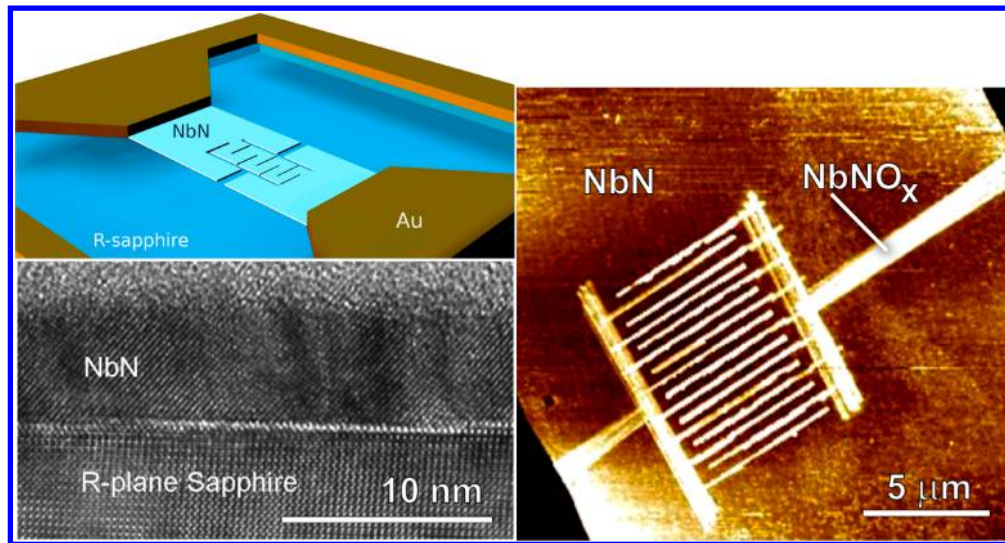


Figure 1. Top left: representation of the whole device showing the superconducting NbN nanowire realized on sapphire substrate, electrically connected to Au leads. Bottom: high-resolution transmission electron micrograph showing a cross-section of a (135) oriented NbN epitaxial layer on R-plane sapphire. Right: atomic force microscope of a 4-nm-thick-NbN meander line realized by local anodization with an atomic force microscope of a 20 μm wide strip line. The topography color scale is 10 nm. The electrically conductive area corresponds to the dark brown surface, which is laterally limited by the strip edges (in black) and locally defined by AFM-patterned insulating NbN-oxide lines (bright lines).

down to very low temperatures (200 mK) (see Supporting Information for details). Figure 2 details the resistance–temperature (R – T) curves of a typical EBL-made nanowire measured under increasing bias current from very low current (4% of critical current, black curve) up to values reaching the critical current (upper curve, brown). Despite the high crystalline quality of the nanowires, the superconducting transition is wide, and a residual resistance remains down to temperatures well below the superconducting transition temperature (T_c). The resistive tail has been observed for different nanowires either made using AFM or using e-beam nanolithography.

At low bias current (below $I_c/2$), the resistance–temperature curve shows a fluctuation-governed transition (black curve, Figure 2a). These fluctuations are of two kinds. Just above T_c , they originate from amplitude fluctuations of the order parameter that locally deplete the density of Cooper pairs (n_s). Correction to the conductivity depends on the superconductor dimension.¹⁴ Although we have to note that the nanowire width is larger than the coherence length ξ of NbN, the 1D-model provides the most consistence with our data. Figure 2b provides a fit of the resistance–temperature curve with the extended 1D of the Aslamasov–Larkin model¹⁴ valid above T_c :

$$(R^{-1} - R_n^{-1})^{-1} = N_c \times \frac{32}{\pi^2} \left(\frac{\hbar}{4e^2} \right) \frac{w}{\xi(0)} \left(\frac{T}{T - T_c} \right)^{-3/2} \quad (1)$$

with R_n as the normal resistance of the nanowire (365 k Ω), w the nanowire width (100 nm), and N_c the number of squares ($L/w = 400$). From the fit, we estimate similar values of $T_c = 11.63$ K and $\xi(0) = 6$ nm to those reported previously.^{15,16}

At lower temperatures, phase fluctuations become the main source of noise. Phase slippages can be thermally or quantum activated, leading to different temperature dependences of the low bias current properties that can be precisely modeled. Little's model¹⁷ allows us to estimate the contribution of thermally activated phase slips (TPS) as function of the ratio

between the superconducting condensation energy ΔF and the thermal energy $k_B T$:

$$R_{\text{TPS}}(T) = R_n \exp\left(-\frac{\Delta F(T)}{k_B T}\right) \quad \text{with} \\ \Delta F(T) = 0.83 k_B T_c \frac{R_q}{\rho} \frac{wd}{\xi(0)} \left(1 - \frac{T}{T_c}\right)^{3/2} \quad (2)$$

Figure 2c compares the data (black dots) and the model result (TPS curve). All parameters have been iteratively adjusted to converge toward the best agreement. The same values of $\xi(0)$, w , and d (respectively 6 nm, 100 nm, and 4 nm) as eq 1 are used with $\rho = 22 \mu\Omega\text{-cm}$, while T_c (11.76 K) and the involved normal resistance R_n (200 k Ω) are slightly different.

For lower temperatures, the TPS model fails to describe the residual resistance. As predicted^{5,6} and observed experimentally,¹⁸ the QPS activated regime should be reached soon after T_c (70% of T_c). To estimate their contribution on the low-temperature side of the R – T curve, we use the model developed by Golubev et al.^{19,20} valid in the dirty limit ($l < \xi$):

$$R_{\text{QPS}}(T) = BR_q S_{\text{GZ}} \frac{L}{\xi(T)} \exp(-S_{\text{GZ}}) \quad \text{with} \\ S_{\text{GZ}} = C \frac{R_q}{R_n} \frac{L}{\xi(T)} \quad (3)$$

according to the following expression of the superconducting coherence length:

$$\xi(T) = 0.907 \xi(0) \left(1 + (1 - 0.25t) \frac{\xi(0)}{t}\right)^{-1/2} \\ \times (1 - t^2)^{-1/2} \quad \text{with} \quad t = T/T_c \quad (4)$$

After several iterations made to adjust the fitting parameters, the fit provides an accurate agreement with the resistive tail and the model in this temperature range (Figure 2c), showing a crossover between QPS and TPS regimes. The fitting QPS

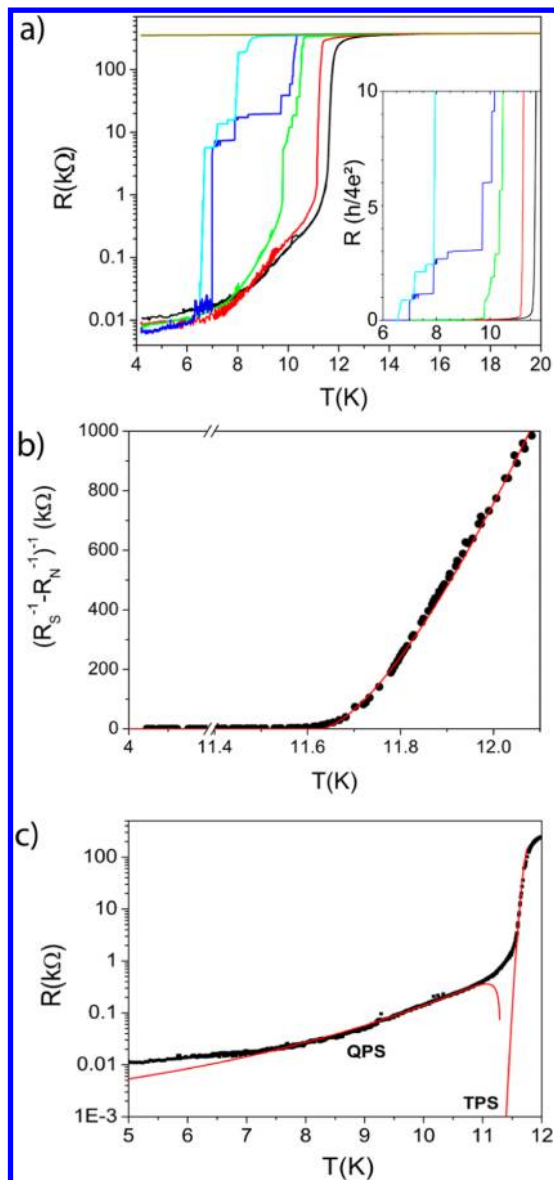


Figure 2. Resistance temperature curves for 100-nm-wide NbN nanowire. (a) R – T plotted in a semilog-scale to emphasize the residual resistance fluctuations below T_c measured under increasing bias currents, from right to left: 1, 5, 10, 15, 20, and 25 μA . Inset: magnification of the superconducting region of the same data plotted in units of quantum resistance ($6.45 \text{ k}\Omega$). (b) Temperature dependence of the invert of paraconductivity $(R_s^{-1} - R_n^{-1})^{-1}$ at temperatures near the critical temperature T_c . Current biasing of the nanowire is performed under low DC current 1 μA (4% of I_c). Data are compared with 1D model (solid red line) calculated using eq 1 (see text). Fitting parameters are detailed in the text. (c) Fits of the R – T curve at low current bias (ca. 4% of I_c) using both thermal (TPS) and quantum (QPS) phase slips models using eqs 2 and 3, respectively. Fitting parameters are in the text.

curve is obtained with $L = 30 \mu\text{m}$, $l = 3.5 \text{ nm}$ as the mean free path, $B = 0.0001$ and $C = 0.047$, assuming deviations on T_c (11.3 K) and the involved normal resistance R_n (280 k Ω) when compared to the previous fits (see eqs 1 and 2). R_n varies abruptly at the transition (5 orders of magnitude) and could be strongly affected by small fitting errors on T_c . Local inhomogeneities could also change the normal length involved in the dissipative regimes, showing different sensitivity to local

disorder. Moreover, at the lowest temperatures, the QPS model does not explain the residual resistance, which reaches almost 10 Ω . This value is much lower than the square resistance of the wire (about 900 Ω) and does not depend of the bias current. It appears more related to the Au-pads that could add a low contact resistance in series with the sample (see the representation in Figure 1, top left).

Phase slips have been underlined even in thicker (50 nm) NbN nanowires.²¹ Their occurrence can be reduced or even suppressed by lowering the current biasing.^{22,18} In fact, both current and temperature reduce the superconducting condensation energy and increase the phase slip rate that depends on the probability to overcome this energy barrier²³ (eqs 2 and 3). First considered as a source of noise, phase slips appear useful for quantum detection,⁷ and their stability against hotspot formation²⁴ is crucial for current bias operation. Hotspot involves Joule heating and longer relaxation times compared with phase slips that should allow keeping the lowest dead time for single photon detection (ps).

A high bias current induces a set of discrete and quantized resistance drops that become more distinct as the current bias increases (Figure 2a and inset). Some resistive steps occur at the same temperature. This particular step-structure has been reported 22 years ago²⁵ in tin whiskers and identified later as phase slip centers (PSC). At the PSC position, the supercurrent periodically reaches the critical current and oscillates at the Josephson frequency¹⁴ (defined as $\nu = 2eV/h$) between 0 and I_c to maintain a nonzero time average supercurrent even over I_c . PSCs could originate from sample inhomogeneities that might be induced by nanolithography processes. PSCs have indeed been reported even in the monocrystalline tin wires (such as whiskers).²⁶

Similar resistive steps are measured in the current–voltage (I – V) curves. They are compared in Figure 3a for both current (red line) and voltage biases (blue dots). One interesting feature lies in the resistive jumps occurrence. Similarly, regular current–voltage steps are found for both biases. Slopes converge all to a nonzero time average supercurrent almost the same as the quasiparticles current, such as $\langle I_s \rangle = I - \langle I_{qp} \rangle \sim I_c/2$. This behavior is well-explained with the theoretical framework based on PSCs such as the SBT model.²⁷ Originally restricted to purely one-dimensional superconductors, PSCs were reported in wider superconducting wires,²⁸ and the models were extended phase slip lines (PSL)^{29,30} for 2D or quasi 1D superconductors.

When temperature is lowered, voltage steps become more distinct. By extrapolation at zero voltage slopes of the linear part following the steps converge to a constant value I_s which equals about $I_c/2$ (Figure 3b). These steps are also the clear signatures of PSCs as averaged in time the supercurrent is limited by its critical value in the phase slip which is known to reach typically half the maximum critical current.¹⁴ They remain stable for a current bias, and the formation of hotspot is not observed in the temperature range reached in this experiment (down to 200 mK).

PSCs are governed by the diffusion and relaxation of quasiparticles and by the dynamics of superconducting order parameter in the PSC core.¹⁴ Voltage drops are more intense as temperature is lowered (Figure 3b) in respect with higher QPS diffusion length.²⁵ Similar behavior is found by applying a magnetic field perpendicular to the nanowire (Figure 3c). The step structure is qualitatively unchanged in the (I – V) curve, but their amplitude decreases while increasing the magnetic field.

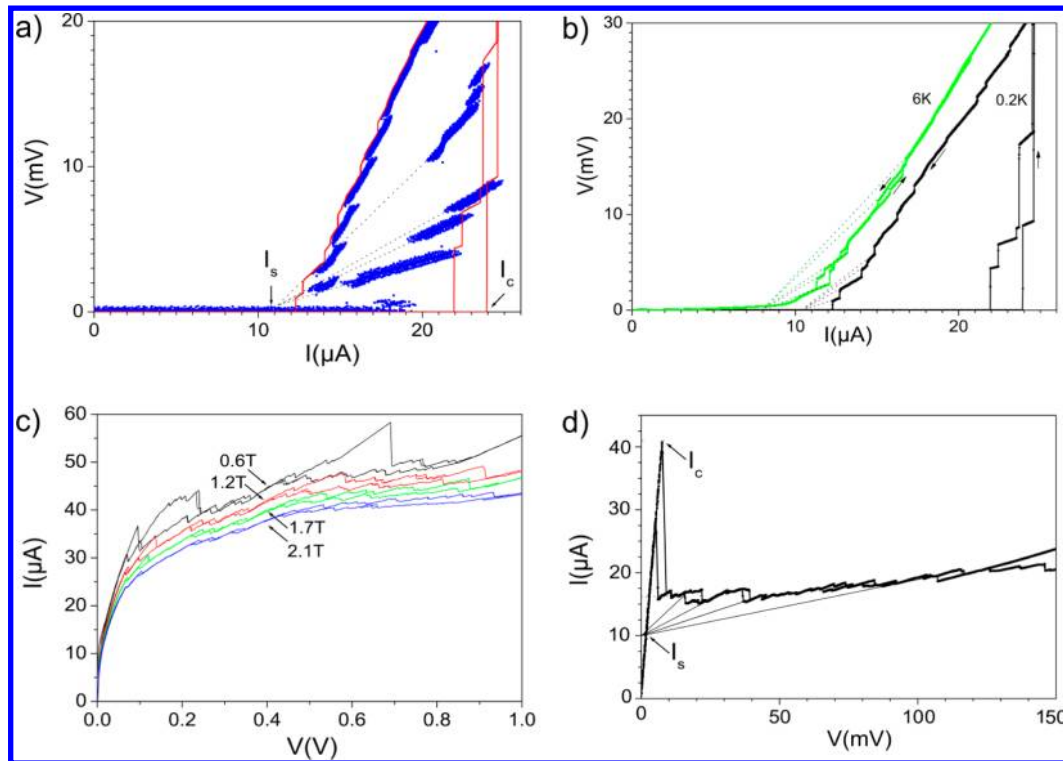


Figure 3. Current–voltage characteristics of the NbN nanowire. (a) (I – V) curves under current (red line) and voltage bias (blue dots) at 200 mK. (b) Temperature dependence of current bias (I – V) curves, $T = 200$ mK and 6 K (respectively, $0.02T_c$ and $0.7T_c$). (c) Voltage biased (I – V) curves for increasing magnetic field B applied perpendicular to the sample. From top to bottom $B = 0.6, 1.2, 1.7,$ and 2.1 T. (d) Zoom near I_c of the voltage biased (I – V) curve at 4.2 K.

As a well-known pair breaking perturbation, the magnetic field affects the decoherence time of the Cooper pair and thus the spread of the PSCs.^{31,32}

Another interesting behavior is seen in the voltage-biased curve that shows typically the establishment of a constant current region as the voltage increases across the superconducting gap. Accurate measurements in this voltage range at 4.2 K (Figure 3d) show that resistive steps still occur in this particular region and converge to a nonzero time average superconducting current. The constant-current region in the (I – V) curve does not correspond to the spreading of an expected hotspot² but involves more a sequence of localized regions within the nanostructure. Phase slips occur periodically in time and are activated one after the other, as the bias increases until reaching the full transition of a single meander arm.

The photoinduced voltage generated across the illuminated nanowires is measured using RF lock-in detection. Illumination is provided by three high bandwidth light emitting diodes (LEDs) with a peak emission respectively centered in the near-infrared (900 nm), visible (white emission 400–800 nm), and near-ultraviolet (max. emission at 400 nm; see the Supporting Information for details).

The principle of operation of superconducting single photon detectors (SSPDs) are commonly based on the spread of a current assisted hotspot expected at low temperatures when phase slips become unstable.^{24,33} In highlight of the previous analyses, this regime does not occur at the temperatures reached here (200 mK) that remain below the typical range of temperature for single photon detection (1–4 K).

By measuring the photoinduced voltage signal as a function of bias current for different wavelength illumination (Figure 4),

a change appears in the photonic response upon the irradiation wavelength and the temperature of operation.

For the set of curves corresponding to the highest temperature (4.2 K, Figure 4a), the photovoltage shows for all wavelengths an exponential dependence upon the nanowire bias current in the low current bias regime and a sharp cutoff at the critical current. Interestingly, this cutoff occurs at a bias current that just precedes the onset of a finite voltage measured in the dark (top curve of Figure 4a). This result is consistent with the exponential dependence of the counting rate upon current bias, a feature usually observed in SSPD operated in photon counting measurement modes.^{2,8,34} Compared to the more energetic wavelengths, a very weak response is measured upon infrared irradiation. This weak dependence was also observed in SSPD measured in photon counting modes,^{34–36} for which the detector was found only sensitive to two-photon irradiation in the infrared.

A completely different behavior for the spectral dependence of the photoresponse is observed at the lowest temperatures (1.2 K, Figure 4b). While the photon detectivity is somewhat weaker in the visible and UV range and its dependence upon current bias not as sharp, especially at the cutoff, one has to note that the detectivity in the infrared is much improved compared to the higher temperature regime. The spectral dependence of SSPD is indeed shown to be much weaker at low temperatures,³⁷ as more energy is needed to reach the transition point and generate a photovoltage. Further study will tell if the change of spectral sensitivity coincides with the crossover from thermal activation toward the quantum regime for which the incident wavelength should have a weaker effect on phase slip activation.

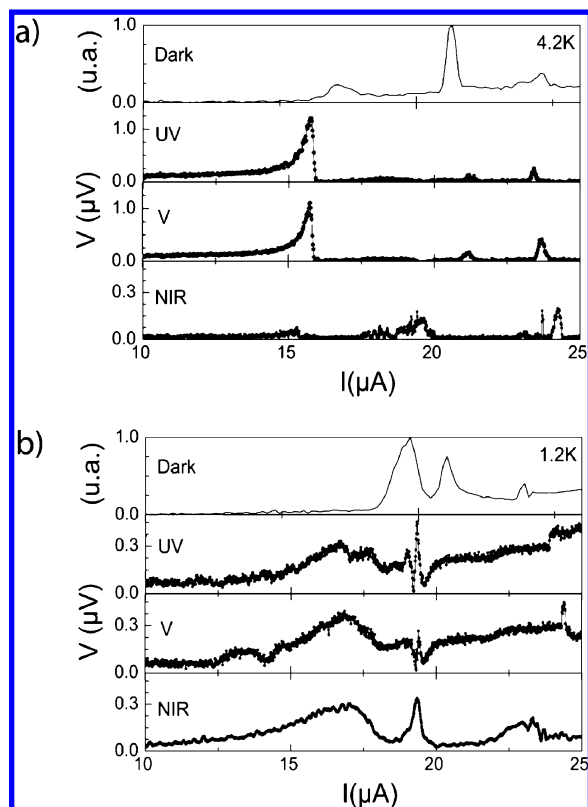


Figure 4. Photoinduced voltage amplitude measured across NbN nanowire as a function of the nanowire bias current at temperatures (a) $T = 4.2$ K and (b) $T = 1.2$ K. Nanowire is successively illuminated with time-modulated ultraviolet ($\lambda_{UV} = 400$ nm), visible ($\lambda_V = 400\text{--}800$ nm), or near-infrared ($\lambda_{NIR} = 900$ nm). The lock-in carrier modulates the light-emitting diode (LED) light intensity at 200 kHz. The top curve (dark) corresponds to the differential resistance of the nanowire without illumination and serves as a reference for the critical current under dark conditions. For those measurements, the bias current is modulated at low frequency (33 Hz) for the lock-in detection.

One SSPD feature that still remains is their low detection efficiency (a few %) that relies mainly on a poor coupling between micronic optical fibers and the nanowires. Resonant coupling cavities have already allowed reaching 60% detection efficiency.³⁸ More recently, new designs have been proposed, based on the particular properties of surface plasmon polaritons to guide photons at the subwavelength scale. Giant evanescent coupling between conventional silicon waveguides and metallic slot waveguides (50 nm) should allow very efficient coupling with the SSPD while being sensitive to the incident polarization useful for cryptographic applications.^{39,40}

In conclusion, due to the ultrathin nature of the wires, we observe signatures of a dissipative regime roughly similar to the one expected for a purely 1D device. They are obtained using different fabrication techniques including an innovative fabrication technique based on local oxidation under the tip of an AFM. The I – V characteristics and temperature dependence show the presence of phase slippages and a crossover from a thermal to quantum activation of these local fluctuations. The absence of a hotspot regime in our system does not affect significantly the photonic response, as its characteristics seem to be consistent to what is usually observed in SSPD, relying on the hotspot regime for the main mechanism of detection. Signatures of these quantum phase

slips have not been reported in similar superconducting single photon detectors,^{9–11} suggesting new insight into photon detection mechanisms in ultrathin film devices.

■ ASSOCIATED CONTENT

Supporting Information

Fabrication (1) and electrical measurements (2) methods. This material is available free of charge via the Internet at <http://pubs.acs.org>.

■ AUTHOR INFORMATION

Corresponding Author

*E-mail: cecile.delacour@grenoble.cnrs.fr.

Notes

The authors declare no competing financial interest.

■ ACKNOWLEDGMENTS

C.D. acknowledges support for a Ph.D. Grant provided by D.G.A. Devices were fabricated using Nanofab facility of Neel Institute, of which the technical team is gratefully acknowledged. We thank J. P. Poizat, J. Claudon, T. Horst, and J. P. Maneval for help and discussions.

■ REFERENCES

- (1) Hadfield, R. H. *Nat. Photonics* **2009**, *3*, 696–705.
- (2) Gol'tsman, G. N.; Okunev, O.; Chulkova, G.; Lipatov, A.; Semenov, A.; Smirnov, K.; Voronov, B.; Dzardanov, A.; Williams, C.; Sobolewski, R. *Appl. Phys. Lett.* **2001**, *79*, 705.
- (3) Zinoni, C.; Alloing, B.; Li, L. H.; Marsili, F.; Fiore, A.; Lunghi, L.; Gerardino, A.; Vakhtomin, Y. B.; Smirnov, K. V.; Gol'tsman, G. N. *Appl. Phys. Lett.* **2010**, *96*, 089901.
- (4) Tarkhov, M.; Claudon, J.; Poizat, J. P.; Korneev, A.; Divochiy, A.; Minaeva, O.; Seleznev, V.; Kaurova, N.; Voronov, B.; Semenov, A. V.; Gol'tsman, G. *Appl. Phys. Lett.* **2008**, *92*, 241112.
- (5) Tinkham, M.; Lau, C. N. *Appl. Phys. Lett.* **2002**, *80*, 2946.
- (6) Bezryadin, A.; Lau, C. N.; Tinkham, M. *Nature* **2000**, *404*, 971–4.
- (7) Mooij, J. E.; Nazarov, Y. V. *Nat. Phys.* **2006**, *2*, 169.
- (8) Delacour, C.; Claudon, J.; Poizat, J. P.; Pannetier, B.; Bouchiat, V.; Espiau de Lamaestre, R.; Villegier, J.-C.; Tarkhov, M.; Korneev, A.; Voronov, B.; Gol'tsman, G. *Appl. Phys. Lett.* **2007**, *90*, 191116.
- (9) Semenov, A. D.; Haas, P.; Hübers, H.-W.; Ilin, K.; Siegel, M.; Kirste, A.; Schurig, T.; Engel, A. *Physica C (Amsterdam, Neth.)* **2008**, *468*, 627–630.
- (10) Bartolf, H.; Engel, A.; Schilling, A.; Il'in, K.; Siegel, M.; Hübers, H.-W.; Semenov, A. *Phys. Rev. B* **2010**, *81*, 024502.
- (11) Hofherr, M.; Rall, D.; Ilin, K.; Siegel, M.; Semenov, A.; Hübers, H.-W.; Gippius, N. A. *J. Appl. Phys.* **2010**, *108*, 014507.
- (12) Villegier, J.-C.; Bouat, S.; Cavalier, P.; Setzu, R.; Espiau de Lamaestre, R.; Jorel, C.; Odier, P.; Guillet, B.; Mechin, L.; Chauvat, M. P.; Ruterana, P. *IEEE Trans. Appl. Superconductivity* **2009**, *19*, 3375.
- (13) Cooper, E. B.; Manalis, S. R.; Fang, H.; Dai, H.; Matsumoto, K.; Minne, S. C.; Hunt, T.; Quate, C. F. *Appl. Phys. Lett.* **1999**, *75*, 3566.
- (14) Tinkham, M. *Introduction to superconductivity*, 2nd ed.; McGraw Hill: New York, 1996.
- (15) Jones, H. C. *Appl. Phys. Lett.* **1975**, *27*, 471.
- (16) Shoji, A.; Kiryu, S.; Kohjiro, S. *Appl. Phys. Lett.* **1992**, *60*, 1624.
- (17) Little, W. A. *Phys. Rev.* **1967**, *156*, 396.
- (18) Rogachev, A.; Bezryadin, A. *Appl. Phys. Lett.* **2003**, *83*, 512.
- (19) Zaikin, A. D.; Golubev, D. S.; van Otterlo, A.; Zimanyi, G. T. *Phys. Rev. Lett.* **1997**, *78*, 1552.
- (20) Golubev, D. S.; Zaikin, A. D. *Phys. Rev.* **2001**, *B 64*, 014504.
- (21) Elmurodov, A. K.; Peeters, F. M.; Vodolazov, D. Y.; Michotte, S.; Adam, S.; de Menten de Horne, F.; Piraux, L.; Lucot, D.; Mailly, D. *Phys. Rev. B* **2008**, *78*, 214519.

- (22) Bell, M.; Sergeev, A.; Mitin, V.; Bird, J.; Verevkin, A.; Gol'tsman, G. *Phys. Rev. B* **2007**, *76*, 094521.
- (23) Bezryadin, A. *J. Phys.: Condens. Matter* **2008**, *20*, 043202.
- (24) Maneval, J.-P.; Boyer, F.; Harrabi, K.; Ladan, F.-R. *J. Superconductivity* **2001**, *14*, 347.
- (25) Tidecks, R. *Current-Induced Nonequilibrium Phenomena in Quasi-One-Dimensional Superconductors*; Springer: Berlin, 1990.
- (26) Meyer, J. D.; Minnigerode, G. V. *Phys. Lett. A* **1972**, *38*, 529.
- (27) Skocpol, W. J.; Beasley, M. R.; Tinkham, M. J. *Low Temp. Phys.* **1974**, *84*, 289.
- (28) Sivakov, A. G.; Glukhov, A. M.; Omelyanchouk, A. N.; Koval, Y.; Müller, P.; Ustinov, A. V. *Phys. Rev. Lett.* **2003**, *91*, 267001.
- (29) Weber, A.; Kramer, L. *J. Low Temp. Phys.* **1991**, *84*, 289.
- (30) Volotskaya, V. G.; Dmitrenko, I. M.; Sivakov, A. G. *Soviet J. Low Temp. Phys.* **1984**, *10*, 179.
- (31) Kadin, A. M.; Skocpol, W. J.; Tinkham, M. J. *Low Temp. Phys.* **1978**, *33*, 481.
- (32) Schmid, A.; Schön, G. *J. Low Temp. Phys.* **1975**, *20*, 207.
- (33) Adam, S.; Piraux, L.; Michotte, S.; Lucot, D.; Mailly, D. *Superconducting Sci. Technol.* **2009**, *22*, 105010.
- (34) Verevkin, A.; Zhang, J.; Sobolewski, R.; Lipatov, A.; Okunev, O.; Chulkova, G.; Korneev, A.; Smirnov, K.; Gol'tsman, G. N.; Semenov, A. *Appl. Phys. Lett.* **2002**, *80*, 4687.
- (35) Maingault, L.; Tarkhov, M.; Florya, I.; Semenov, A.; Espiau de Lamaestre, R.; Cavalier, P.; Gol'tsman, G.; Poizat, J.-P.; Villegier, J.-C. *J. Appl. Phys.* **2010**, *107*, 116103.
- (36) Semenov, A. D.; Haas, P.; Günther, B.; Hübers, H.-W.; Il'in, K.; Siebel, M. *J. Low Temp. Phys.* **2008**, *151*, 564.
- (37) Milostnaya, I.; Korneev, A.; Tarkhov, M.; Divochiy, A.; Minaeva, O.; Seleznev, V.; Kaurova, N.; Voronov, B.; Okunev, O.; Chulkova, G. *J. Low Temp. Phys.* **2008**, *151*, 591.
- (38) Gol'tsman, G.; Minaeva, O.; Korneev, A.; Tarkhov, M.; Rubtsova, I.; Divochiy, A.; Milostnaya, I.; Chulkova, G.; Kaurova, N.; Voronov, B.; Pan, D.; Kitaygorsky, J.; Cross, A.; Pearlman, A.; Komissarov, I.; Slysz, W.; Wegrzecki, M.; Grabiec, P.; Sobolewski, R. *IEEE Trans. Appl. Superconductivity* **2007**, *17*, 246.
- (39) Delacour, C.; Blaize, S.; Grosse, P.; Fedeli, J. M.; Bruyant, A.; Salas-Montiel, R.; Lerondel, G.; Chelnokov, A. *Nano Lett.* **2010**, *10*, 2922.
- (40) Delacour, C.; Tchel'nikov, A.; BenBakir, B.; Fedeli, J. M. Patent WO/2011/070,249, 2011, France. Delacour, C. Patent Specification WO/2012/052, 628, 2012, France.